Looking inside the rotating red giant star KIC 614777 by means of asteroseismology with *Kepler*

Dumitru Pricopi, Marian Doru Suran, Diana Constantin

Abstract. We have analysed oscillations of the red giants star KIC 6144777 observed by NASA *Kepler* satellite. The data consists of the first eleven quarters of science operations of *Kepler* which cover about 27 months. The high signal-to-noise ratio (S/N) and continuous data sets allow us to accurately extract the oscillation parameters from the power spectrum. We have found that the mean large frequency separation, $\Delta\nu$, and the frequency of the maximum oscillation power, νmax, are around 10.9 and 128 μHz, respectively. We use the scaling relations of $\Delta\nu$ and $\nu_{\max}$ to estimate the preliminary asteroseismic mass, which will be compared with results of detailed stellar modeling. Stellar models are calculated with CESAM2k stellar evolution code. We have calculated the oscillation frequencies of p mode of degree l up to *3* and the frequencies of a large number of models along the evolutionary tracks using LNAWENR linear, non-radial, non-adiabatic oscillation code. We have chosen the KIC values to constrain the effective temperature, metallicity and surface gravity of the best fitting model of KIC 6144777. We have measured the observed rotational splittings in the nonradial dipole mixed modes and we have found the maximum value of the rotational splitting in the g-m mixed modes as 0.237 μHz. The link between observed rotational splittings and the rotating core is investigated. By fitting a model of internal rotation profile to observed splittings we have estimated the size of rigid rotating core as about 0.004 of stellar radius. Also, we have found differential rotation in the convective envelope as a signature of angular momentum transport from core to envelope. The mean observational period spacing for the l=1 mixed modes of about 61 s suggests that this red giant branch star is in the shell hydrogen-burning phase.

1. INTRODUCTION

Asteroseismology represents the only method that we know today to probe the stellar interior. In the past decade, the asteroseismology of red giants has developed rapidly. The successfully detection of solar like oscillations in G- and K-type giants based on ground-based observations (Frandsen et al. 2002; De Ridder et al. 2006; Stello et al. 2007) and on space-based photometry detections observed by the *Hubble Space Telescope* (Edmonds & Gilliland 1996; Gilliland 2008; Stello & Gilliland 2009), *WIRE* (Buzasi et al. 2000; Retter et al. 2003; Stello et al. 2008), *SMEI* (Tarrant et al. 2007), *MOST* (Barban et al. 2007; Kallinger et al. 2008a, 2008b), *CoRoT* (De Ridder et al. 2009; Hekker et al. 2009; Carrier et al. 2010; Mosser et al. 2010), and *Kepler* (e.g., Bedding et al. 2010; Huber et al. 2010; Kallinger et al. 2010; Hekker et al. 2011a, 2011b; Di Mauro et al. 2011; Chaplin et al. 2010, 2011) led to a rapidly increasing of our knowledge about their internal structure and oscillation properties by using the techniques of asteroseismology (Aerts et al. 2010, Christensen-Dalsgaard 2004, Christensen-Dalsgaard et al. 2007; Gilliland et al. 2010). Red giants are characterized by a deep convective envelope and a small degenerate helium core. The detected solar-like nonradial oscillations by *CoRoT* and *Kepler* satellites are mixed modes that act as high order g-modes in the centre and as low order p-modes in the

outer convective region (Guenther et al. 2000; Dziembowski et al. 2001; Teixeira et al. 2003; Christensen-Dalsgaard 2004).
The long and uninterrupted photometric time series of red giants provided by the space mission *Kepler* allow us to probe the rotational behaviour in their deep interiors using the observations of mixed modes. The red giants are expected to have a rapidly rotating core and a slowly rotating envelope (e.g. Sills & Pinsonneault 2000), as a result of internal angular momentum distribution. Mosser et al. (2012) have measured rotational splittings in a sample of about 300 red giants and have shown that these splittings are dominated by the core rotation. They also developed a dedicated method for automated measurements of the rotational splittings in a large number of red giants.
We analyze in this work the star KIC 6144777, which is a bright red giant in the *Kepler* field ($V = 10.687$). Observations and data are presented in Section 2. The oscillation parameters are estimated in Section 3. The observed rotational splittings are compared with those predicted by the model of Mosser et al (2012). Section 4 deals with stellar modelling, and a model of KIC 6144777 is presented. The way the measured rotational splitting is related to the core rotation is quantified. An analytical model of the internal rotation profile is proposed as a tool to investigate the transport of angular momentum from core to envelope and to estimate the size of the rigid rotating core. Concluding remarks end this paper.

2. OBSERVATIONS

KIC 6144777 has been observed by the Kepler satellite (Borucki et al. 2008, 2010; Koch et al 2010) during the Q0 – Q10 runs in long cadence mode. The Kepler long cadence observation mode corresponds to an integration time of 29.4 minutes (Jenkins et al. 2010) and a Nyquist frequency of 283 μHz. The data that we describe here were obtained during 823 days, starting on 2009, May 02 and ending on 2011, September 28. The raw photometric data were reduced by Kepler team as described in the "Data Release Notes" (http://archive.stsci.edu/kepler/data_release.html). For red giants, the data were corrected for slopes and discontinuities by Saskia Hekker (see KASOC Data Release webpage, http://kasoc.phys.au.dk/index.php). The top panel of figure 1 shows the cleaned light curve normalized to mean value after discarding obvious outliers.

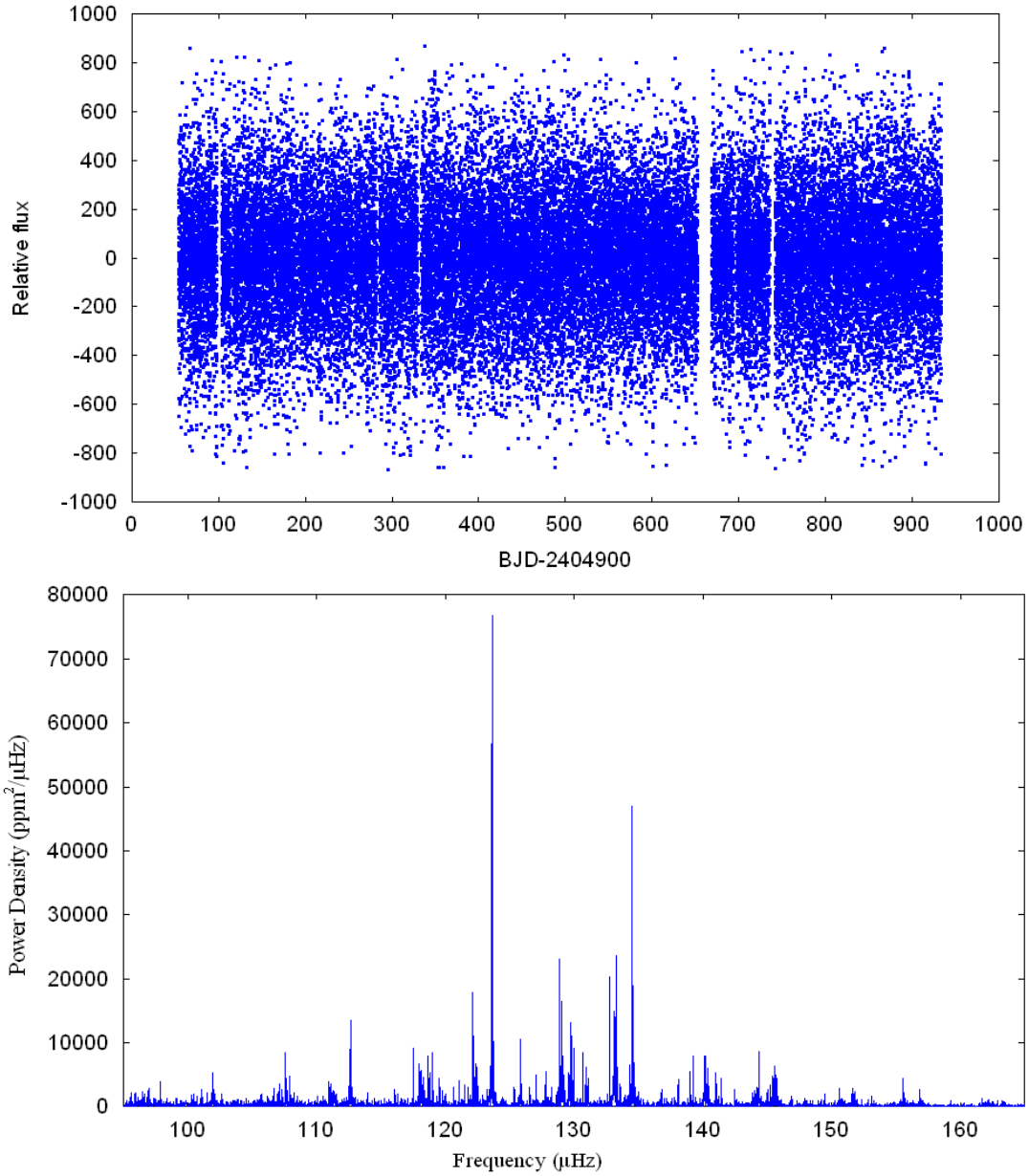

Figure 1. . Top panel: Light curve corrected for slopes and discontinuities, cleaned for obvious outliers and normalized to the mean value. Bottom panel: Power Spectrum Density in the region of p mode excess hump.

3. GLOBAL OSCILLATION ANALYSIS

The unprecedented quality of *Kepler* observations allow us precise measurements of solar-like oscillations detected in RGs. Power spectra is used to extract frequencies, amplitudes, mode energy, and mode lifetime. From the power spectrum we will identify the order and degree of a given solar-like oscillation mode through the p-mode structure of solar-like oscillations seen in the power excess region. The mode identification is crucial for any comparison between a stellar model and the observed oscillation frequencies (see next section). As is well known, in a solar-like star the solar-like oscillations are usually high-order low-degree p-modes. Their frequencies

are regularly spaced, approximately following the asymptotic relation (Tassoul 1980, Gough 1986):

$$\nu_{n,l} \approx \Delta\nu(n + l/2 + \varepsilon) - l(l+1)D_0$$

where l is the mode degree, n is the mode order, $\Delta\nu$ is the large frequency separation (is approximately the inverse of the sound travel time across the star). The parameter ε, named in literature the phase offset, comprises two parts (Mosser et al. 2011b): the offset due to the mode propagation in the uppermost layers of the star, and the second-order term of the asymptotic approximation, which is sensitive to the gradient of sound speed in the stellar interior. Finally, D_0 is sensitive to the sound speed gradient near the core. For a red giant star, the solar-like oscillations with mode degree $l > 0$ are nonradial oscillations that have a mixed character, behaving like high-order g-modes in the core and low-order p-modes in the envelope. They undergo so-called *avoided crossings* (Osaki 1975; Aizenman et al. 1977) that lead to a shift in frequency. An asymptotic relation similar to (1) was derived for mixed modes in red giants (Huber et al. 2010; Mosser et al. 2011).

Our frequency analysis covers few basic steps that are performed on the power spectrum of the Kepler light curve: modelling the background signal by fitting with a model, estimating the frequency of maximum power ($\nu_{\max}$), estimating the large separation ($\Delta\nu$) and calculating the $l = 0,1,2,3$ centroids in the collapsed power spectrum, calculating the small separations according to Huber et al (2010), calculating and fitting the rotational splitting observed for dipole modes using the asymptotic relation of Mosser et al (2011), extracting individual mode frequency, mode lifetime and height by fitting the p-mode region of the power spectrum with a sum of Lorentzian profiles. In the following subsections we describe these analysis steps in detail.

3.1. MODELLING THE BACKGROUND AND DETERMINING $\nu_{\max}$

The power spectrum shows a frequency-dependent background signal due to various stellar surface phenomena. In this paper, the signal due to granulation is modelled by a modified Lorentzian-like function, first introduced by Karoff (2008). The contribution of the other surface phenomena (such as stellar activity, faculae, etc.) to background signal is included in a white noise component. The power excess hump from stellar oscillations is approximately Gaussian, so the complete spectrum is modelled by:

$$P(\nu) = P_n + \frac{4\sigma^2\tau}{1 + (2\pi\nu\tau)^2 + (2\pi\nu\tau)^4} + P_g \exp\left(\frac{-(\nu_{\max} - \nu)^2}{2\sigma_g^2}\right), \quad (1)$$

where P_n corresponds to the white noise component, σ is the rms intensity of the granules, τ is the characteristic time scale of granulation. The parameters P_g, $\nu_{\max}$ and σ_g are the height, the central frequency and the width of the Gaussian profile that model the power excess hump. The component of background and the white noise were simultaneously fitted to power spectrum outside the region where the power excess hump is seen. For the fitting of the power density spectrum of KIC006144777 with the model given by Equation (1) we used Maximum Likelihood Estimator (Appourchaux 2003). The fit returned, among other parameters, the maximum

amplitude of excess power $P_{max} = 867.406 \pm 23.079 \mathrm{ppm}^2 \mu\mathrm{Hz}^{-1}$. The corresponding frequency is $\nu_{max} = 128.803 \pm 2.598 \mu\mathrm{Hz}$ (Figure 2).

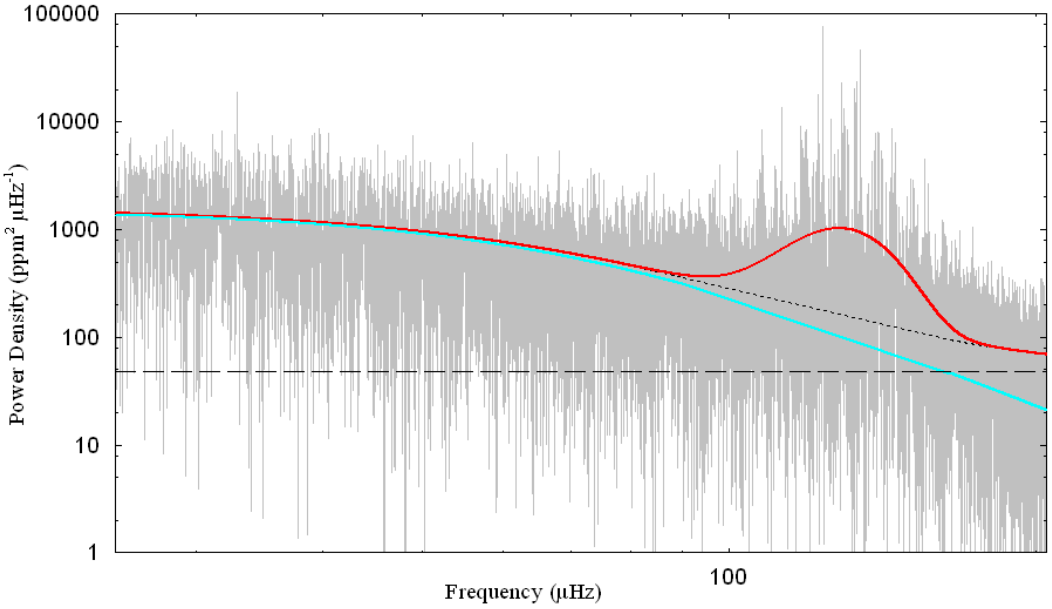

Figure 2. Power density spectrum of KIC 6144777. Light grey: power density spectrum, thick solid red line: global fit according to the model described in the text; dotted line: semi-Lorentzian plus the white noise component, thick solid blue and dashed lines: the semi-Loretzian and the white noise component of the global fit, respectively.

3.2. INDIVIDUAL FREQUENCIES

The bottom panel of Figure 2 shows the power density spectrum in the region of the power excess hump. We see the clear signature of solar-like oscillations: a regular series of peaks spaced by a large separation. We also see multiple peaks due to mixed l=1 and l=3 modes (Beck et al. 2011; Bedding et al 2011). The signature of the rotational splitting is obvious and it will be discussed in the next sub-paragraph.

The analysis of the power spectrum was performed by adopting the peak-bagging method based on the fit of Lorentzian profiles to the power density spectrum using Maximum Likelihood Estimators (MLE) (Appourchaux et al. 1998). The power spectrum was smoothed with a Gaussian and the frequencies of the peaks above a threshold that was set at 0.99 confidence were used as initial starting values for the fitting with Lorentzians. We first computed a guess value for the large frequency separation using power spectrum auto-correlation method in the region of p-mode power excess. Then, we have identified the l=0 peaks (and, immediately, the l=2 peaks) in the power spectrum. Because the mode lifetime is so different for the different modes, we used more than one level of smoothing. We first smoothed with a Gaussian with a FHWM=0.25 to get only one peak per l=0 mode. That also give only one peak per l=2 and for the most p-mode like l=1 mode (the one with the most power in it, higher and broader than the l=1 modes in the wings of each l=1 cluster).

For this smoothing we then set a threshold assuming the spectrum follows a χ^2 distribution with 2*N dof (the distribution of white noise in the power spectrum is

χ^2 with 2*N dof where N is the number of independent bins we have smoothed over; this is explained in detail in the paper of Chaplin et al. 2002). Taking into account that we have smoothed the spectrum, the threshold, say of 0.99 confidence, will be at a lower power density value.
Then we smooth again using less smoothing (FWHM=0.024) to make sure we also get the splitting components of l=1 modes that show obvious rotational splitting and the narrower l=1 modes with long lifetimes (for which the rotational splitting is not so evident). Again, taking the amount of smoothing into account to set the threshold correctly (such that it is still at 0.99 confidence).
As shown in Figure 2, energy (or power) of an oscillation mode is not concentrated in a single frequency. The reason for this is the finite lifetime which will result in mode energy being spread over a frequency range. The shorter the mode lifetime the more power will be spread. The power for an oscillation mode will be distributed as a Lorentzian profile for a given observing period (window) which can be parameterized by mode lifetime τ, size of peak H, and frequency ν. The power spectrum in the region of p-mode excess power was modelled as a background noise component similar with that used in Expression (1) and a sum of Lorentzian profiles. Thus, the total power from the stellar oscillations is described as:

$$P(\nu) = P_n + \frac{4\sigma^2\tau}{1+(2\pi\nu\tau)^2+(2\pi\nu\tau)^4} + \sum_{i=1}^{n} L(\tau_i, H_i, \nu_i) \qquad (2)$$

where $L(\tau_i, H_i, \nu_i)$ is the Lorentzian profile for the observing window for a mode lifetime τ_i, size of the peak H_i, and frequency ν_i. The Lorentzian profile is defined as

$$P_{Lorentzian}(\nu) = L(\tau_i, H_i, \nu_i) = \frac{H_i}{1+(2\pi\cdot(\nu-\nu_i)\cdot\tau_i)^2}$$

We have fitted the power spectrum with the model given by expression (2) using MLE method. We decided to fit each component in a multiple of split frequencies as individual non-split peaks assuming no rotation because our code cannot fit differential rotation, which is the case for RGs. But the many closely spaced peaks makes the fitting difficult, and this could make the mode heights and linewidths to be questionables. The fit returned the value of frequency, lifetime, and height for each oscillation mode (see Table 1). The corresponding uncertainties were calculated using Monte-Carlo simulations by generating 1000 'clones' of power spectrum. We also note that the oscillation modes for which the fitted width is lower than spatial resolution of power spectrum was fitted again using the classical sine function by using the software package Period04 (Lenz & Breger 2004). The resulting frequencies and amplitudes are also listed in Table 1 together with their corresponding uncertainties (also derived by means of Monte-Carlo simulations).
The value of the large separation, $\Delta\nu = 10.905 \pm 0.013\mu$Hz, was found by computing the autocorrelation function of the fitted curve times a weight function. The weight function were expressed as a sum of six supergaussian functions, each of them centred in the central frequencies of the l=0 peaks as is illustrated in the top panel of Figure 3. The uncertainty corresponds to spatial resolution in frequency of the power spectrum. We then estimated the value of the phase offset parameter, $\varepsilon = 1.347 \pm 0.749\mu$Hz,

from the asymptotic relation $\nu_{n0} = \Delta\nu(n+\varepsilon)$ for solar-like p-mode radial oscillations, in which the values of the frequencies and the orders of the radial modes reported in Table 1 were replaced.

In order to extract a rough estimate of the global parameters of the star, to be adopted as guess values for the model computation, we adopted the scaling laws provided by Brown et al. (1991), Kjeldsen & Bedding (1995), and Bedding & Kjeldsen (2003), relating the observed mean large frequency separation and $\nu_{\max}$ to the fundamental parameters of the star. We obtained: $M/M_{Sun} = 1.28 \pm 0.16$, $R/R_{Sun} = 5.80 \pm 0.26$, and $L/L_{Sun} = 14.22 \pm 3.74$. We also derived the radial order of the mode with maximum amplitude in the spectrum, $n_{\max} = \nu_{\max}/\Delta\nu - \varepsilon \approx 10$. This latter value is in agreement with the radial order identification of the radial mode reported in Table 1.

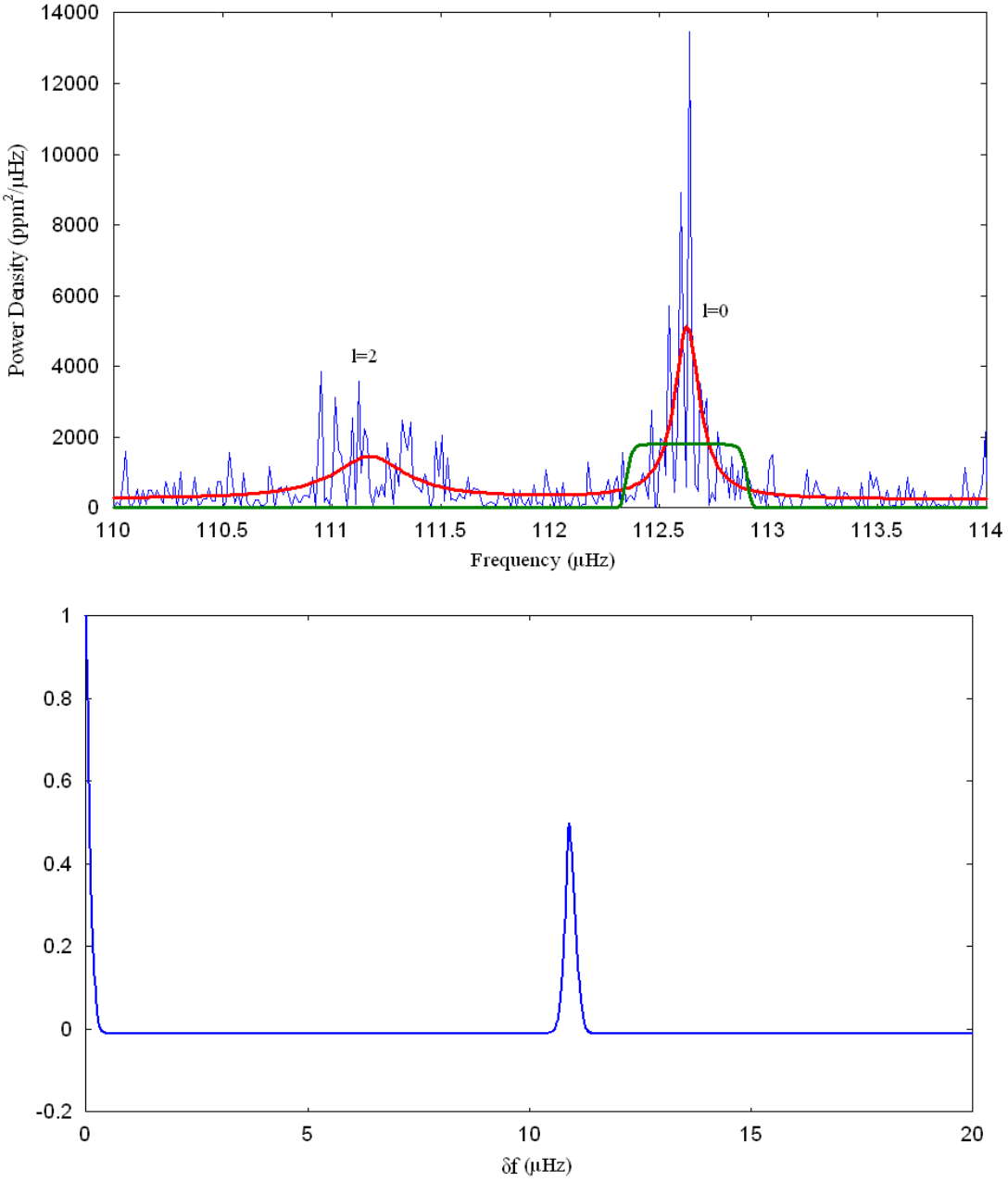

Figure 3. The top panel shows the fitted curve (red), corresponding to expression (2), to the power spectrum (blue). The green line denote the weight function in the region

of the l=0 peak of frequency 112.625 μHz. The bottom panel shows the autocorrelation function calculated for the fitted curve times the weight function. We see a single and strong autocorrelation at the frequency of 10.905 μHz. The large separation, $\Delta\nu$, was set at this value.

As is usual, one may calculate a characteristic set of frequency separations that describes the structure of oscillation frequencies spectrum (Christensen-Dalsgaard, 2004). Observationally, these separations can be expressed as follows (Bedding & Kjeldsen 2010):

$$\nu_{n,l} = \Delta\nu(n + l/2 + \varepsilon) - \delta\nu_{0l} \quad (2)$$

In equation (2), the quantity $\delta\nu_{0l}$ denotes the small frequency separations of non-radial modes relative to radial modes, as follows (Huber et al. 2010):

$$\delta\nu_{02} = \nu_{n,0} - \nu_{n-1,2} \quad (3)$$

$$\delta\nu_{01} = \frac{1}{2}(\nu_{n,0} + \nu_{n+1,0}) - \nu_{n,1} \quad (4)$$

$$\delta\nu_{03} = \frac{1}{2}(\nu_{n,0} + \nu_{n+1,0}) - \nu_{n,3} \quad (5)$$

Following Bedding et al. (2010b), Huber et al. (2010) have used $\delta\nu_{03}$ instead of the more commonly used $\delta\nu_{13}$ due to the broadening of the l = 1 ridge in red giants caused by mixed modes (Dupret et al. 2009; Deheuvels et al. 2010).

To measure the small separations, we have used the technique of Huber et al. (2010). Thus, we first collapsed the power spectrum (Figure 4). We see that, for KIC0061777, the ridges of l=0 and 2 modes can be unambiguously identified. A Gaussian function was fitted to each mode ridge that was identified (Figure 5). The centre of the fitted Gaussian was taken as the position of that ridge. We denote by ν_0, the position of l=0 ridge and by ν_{0l}, the position of l=1, 2 and 3 ridges. The returned values by fitting are: $\nu_0 = 0.336 \pm 0.028$, $\nu_{02} = 0.210 \pm 0.034$, $\nu_{01} = 0.861 \pm 0.067$, and $\nu_{03} = 0.540 \pm 0.046$. Using these values in the Equations (3), (4), and (5), we obtain for the small separations the following values: $\delta\nu_{02} = 0.127 + 0.063/-0.061 \mu$Hz, $\delta\nu_{01} = -0.014 + 0.219/-0.914 \mu$Hz, and $\delta\nu_{03} = 0.307 + 0.198/-0.893 \mu$Hz. In Table 1 are listed the modes frequencies, width and height together with the radial order and degree.

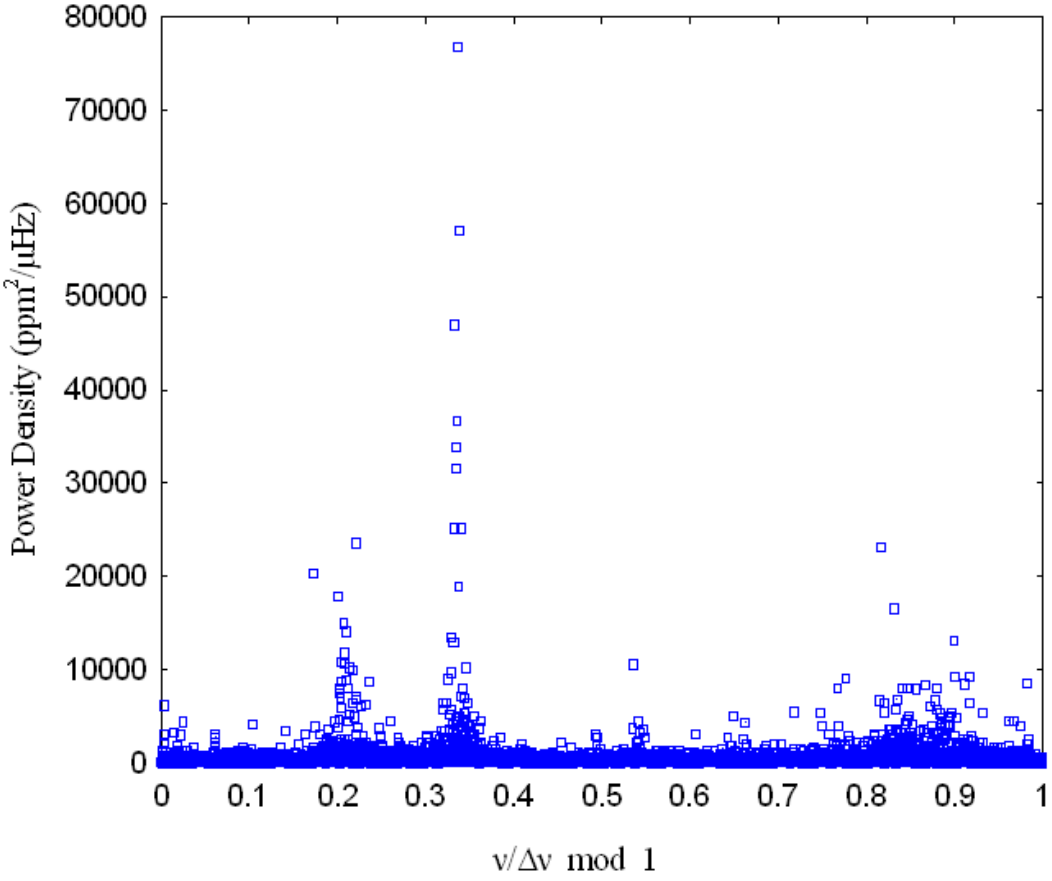

Fig. 4 Collapsed PSD.

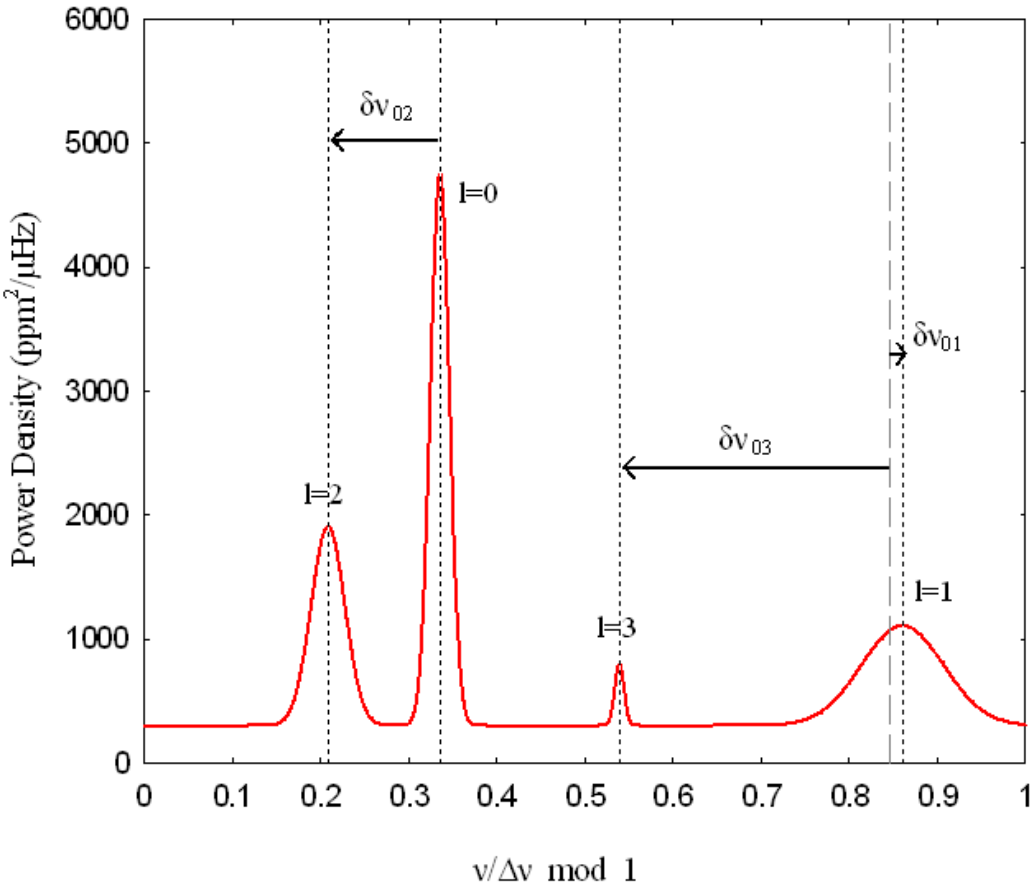

Fig. 5 Ridge identification and definition of small separations used in this paper. The dotted lines mark the centres of l=0, 1, 2, 3 ridge. The dashed line correspond to midpoint of adjacent l=0 modes.

3.3. ROTATIONAL SPLITTING

The power spectrum of KIC 6144777 shows evident rotational splittings. In the case of rotating red giants great care must be taken to disentangle the splittings from the mixed mode spacings. Fortunately, in the case of KIC 6144777, the splittings are small and almost uniform with frequency, except the modulation depicted by R (Eq. 3.3.2), making the estimate straightforward. The unknown stellar inclination can be derived from the mode visibility, which depends on the azimuthal order m. Since l=1 modes seem to show triplets, the inclination angle must be $i \leq 60^{\circ}$ (Gizon et al. 2013). Following Moser et al (2012) we have fitted the rotational splittings with an échelle diagram as a function of the reduced frequency $\nu/\Delta\nu - (n_p + \varepsilon)$ (Fig. 4). Radial modes are centred in 0, quadrupole modes, in -0.137 (with a radial order $n_p - 1$), l=3 modes, in 0.193 and the dipole modes, in 0.514.

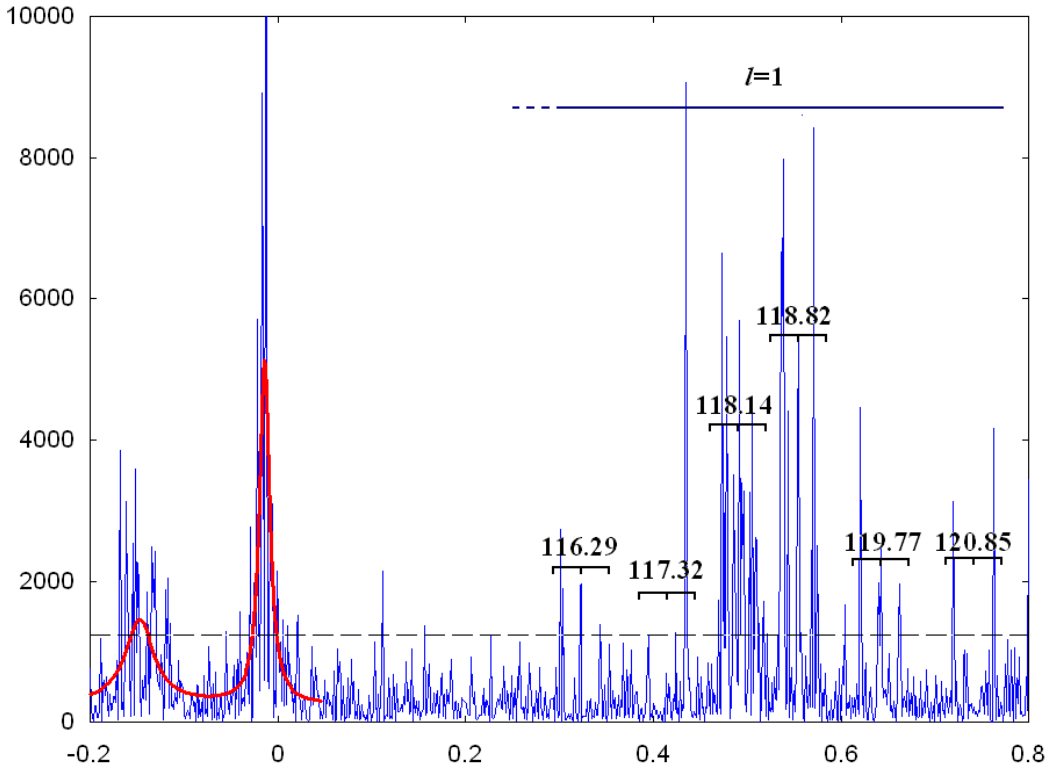
10000
8000
6000
4000
2000
0
-0.2
0
0.2
0.4
0.6
0.8
l=1
118.82
118.14
116.29
117.32
119.77
120.85

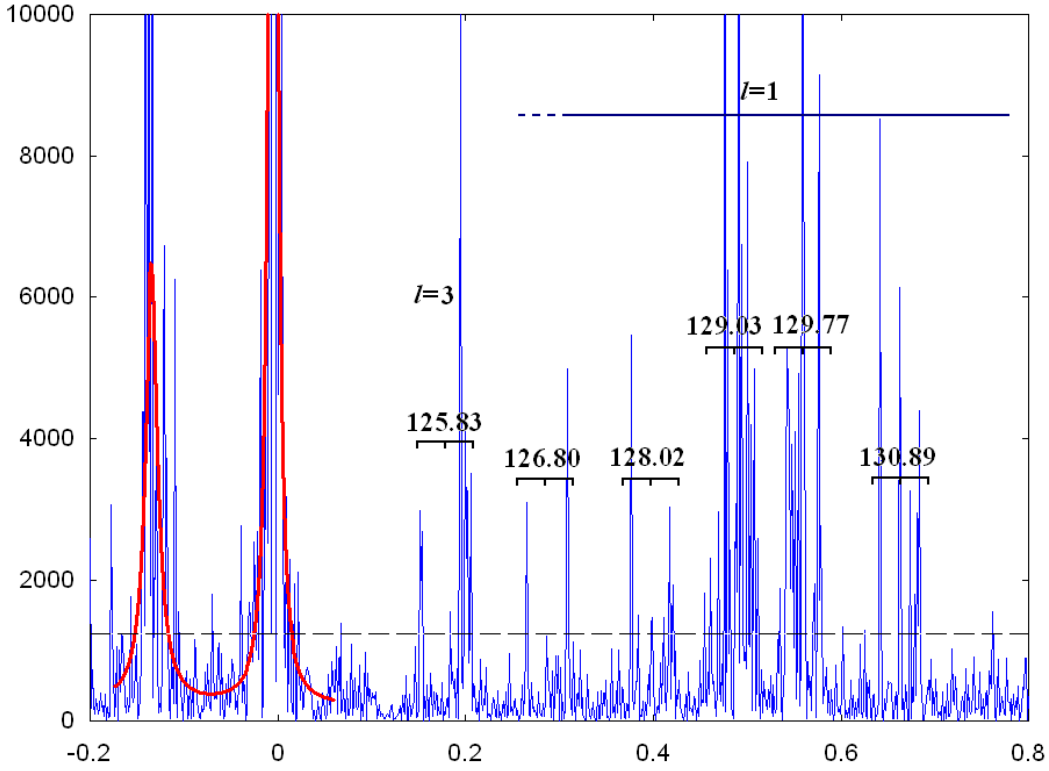
10000
8000
6000
4000
2000
0
-0.2
0
0.2
0.4
0.6
0.8
l=1
l=3
129.03
129.77
125.83
126.80
128.02
130.89

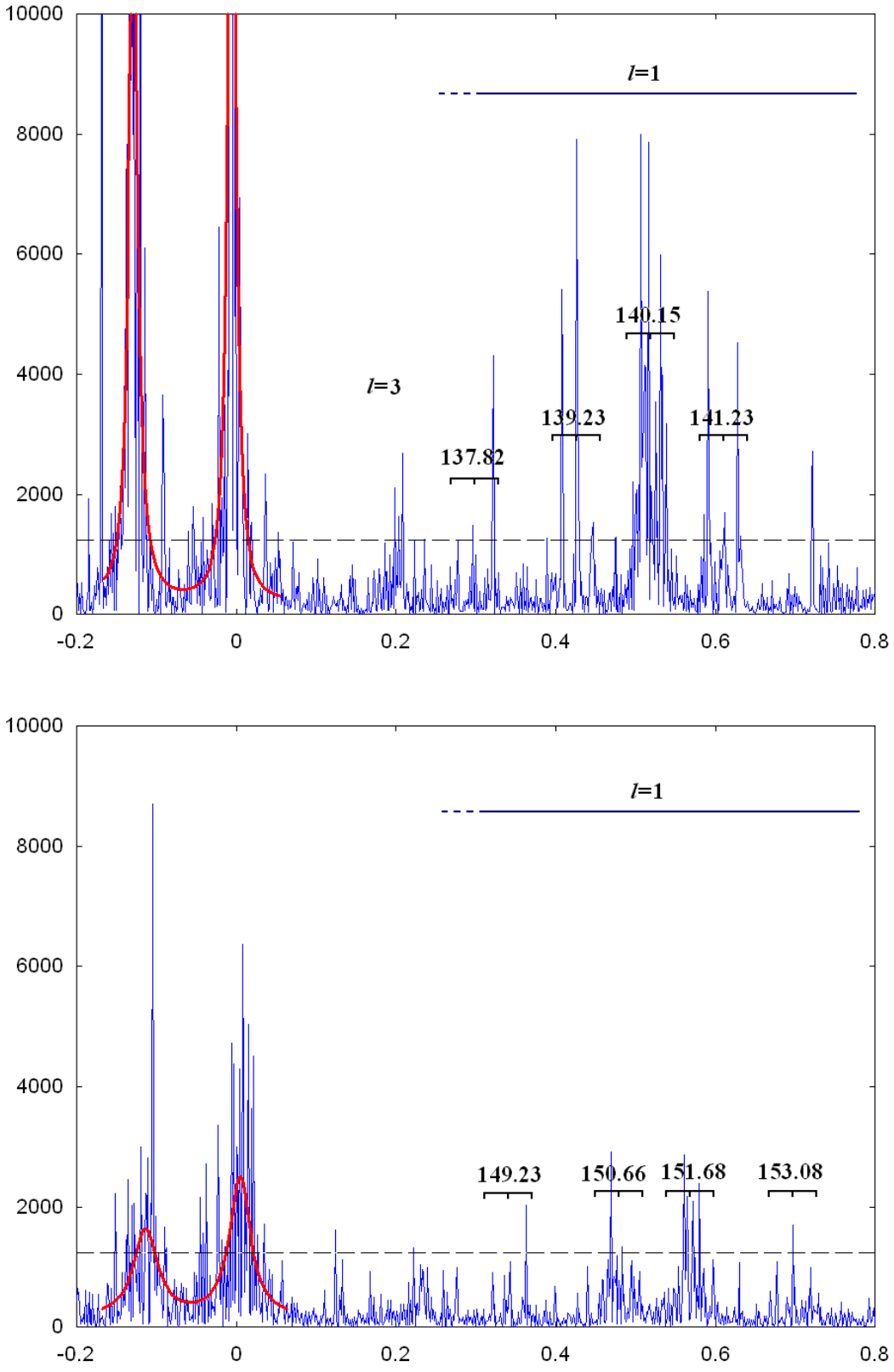

Fig. 6. The échelle diagram as a function of the reduced frequency $\nu/\Delta\nu - (\mathrm{n_p} + \varepsilon)$. The radial order is (from top to down) 9, 10, 11 and 12.

For each triplet we measured the rotational splitting $\delta\nu$ using the autocorrelation method. We computed the autocorrelation function of the smoothed power spectrum times a weight function. The weight function is a supergaussian function centred in the central frequency of a given triplet, as is illustrated in the top panel of Figure 6. For smoothing we used a Gaussian function with FWHM=0.024. For some of the l=1 modes, the splitting components are crystal clear (see the l=1 modes at 119.77 μHz, 130.89 μHz, 141.23 μHz, 153.08 μHz in Figure 4). For these modes is straightforward to compute the rotational splitting $\delta\nu$ (an example is illustrated in Figure 7).

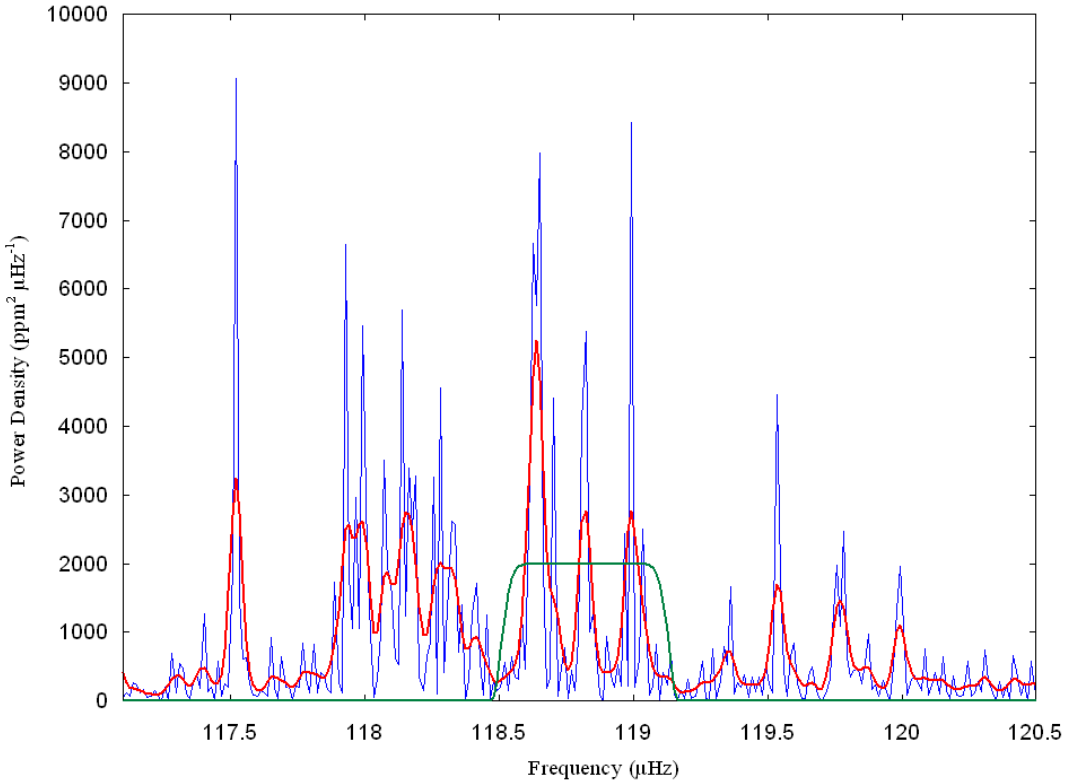

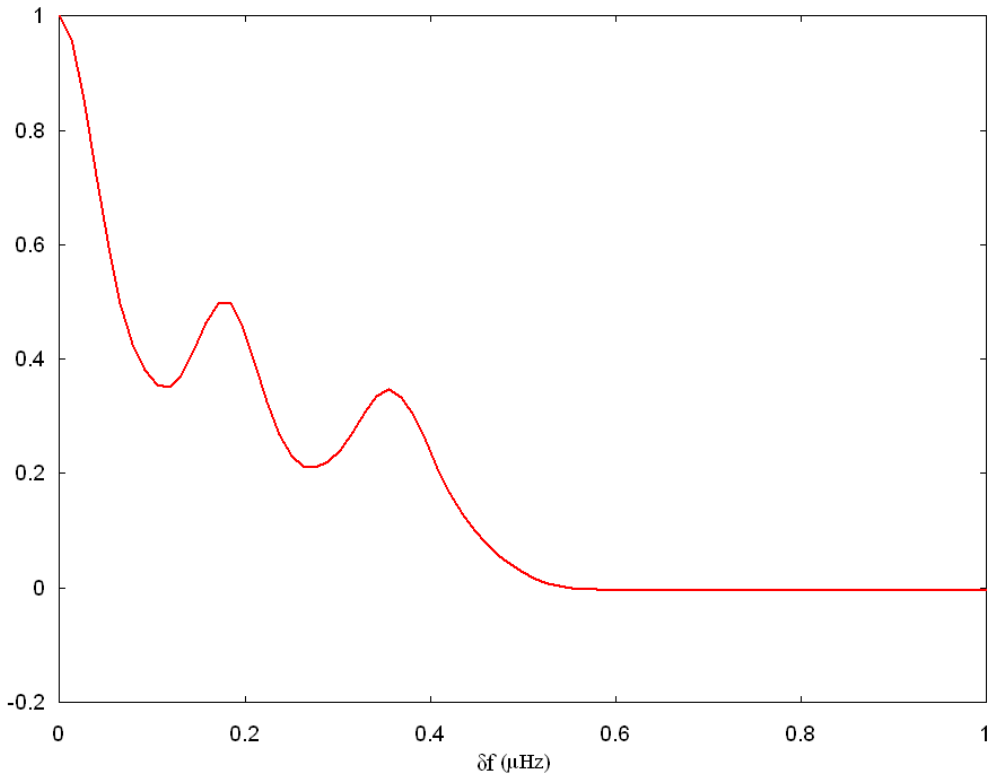

Figure 7. Top panel shows the region of the l=1 modes of the power spectrum (blue) in the frequency range [117, 120] μHz. In order to estimate the rotational splitting, for example, of the l=1 mode situated between 118.5 μHz and 119.2 μHz, we have computed the autocorrelation function of the smoothed power spectrum (red) times the weight function (green) which is a supergaussian function centred in the frequency of the m=0 component, at 118.82 μHz in our case. The bottom panel shows the autocorrelation function. The two peaks correspond to $\delta\nu$ and $2\,\delta\nu$, respectively. We then used the cubic spline interpolation method considering few points around the first peak of the autocorrelation function in order to reduce the uncertainties induced by the spatial frequency resolution (~ 0.0135 μHz) of the power spectrum. The resulting value is $\delta\nu = 0.175\mu$Hz with an uncertainty lower than 10^{-3} μHz.

For many l=1 modes we cannot compute directly the rotational splitting $\delta\nu$ using this method, essentially because of the mode energy distribution between the splitting components. Some of dipolar modes are high and narrower due to their long lifetime, and the splitting components are not so evident (see the l=1 modes at 118.14 μHz, 129.03 μHz, 129.77 μHz, 140.15 μHz, 150.66 μHz, 151.68 μHz in Figure 4). For the others, the m=0 component of the splitting has a very low signal (see the l=1 modes at 117.32 μHz, 120.85 μHz, 126.80 μHz, 128.02 μHz in Figure 4). For these modes, we estimated first $2\delta\nu$, using the autocorrelation method as it was described before. Also, the uncertainties induced by the spatial resolution in frequencies of the power spectrum were reduced under 10^{-3} μHz by using the cubic spline interpolation method considering few points around the peak of the autocorrelation function that corresponds to $2\delta\nu$. The measured values of the rotational splitting for each dipole mode are listed in Table 2. We see that the rotational splittings are modulated in frequency with a period of $\Delta\nu$ which can be explained (Mosser et al 2012) in terms of the interlaced effects of the differential rotation in red giants (Beck et al 2012) and

the mixed nature of the dipole modes that varies as a function of mode frequency (Dupret et al 2009).

Mosser et al (2012) proposed a model for describing the rotational splittings of dipole mixed modes:

$\delta\nu_{split} = \nu_{n,1,m} - \nu_{n,1} = mR_n(\nu)\delta\nu_{rot}$, (3.3.1)

where m is the azimuthal order, $\delta\nu_{rot}$ is the maximum value of the rotational splitting observed for $g-m$ modes, and R is empirically expressed around the position $\nu_{n_p,1}$ of a pure dipole p-mode of radial order n_p as follows:

$$R_{n_p}(\nu) = 1 - \frac{\lambda}{1+\left(\frac{\nu-\nu_{n_p,1}}{\beta\Delta\nu}\right)^2} \quad (3.3.2)$$

for a mixed mode with frequency ν associated with the pressure radial order n_p. The whole frequency pattern of pure p-modes is approximated by (Mosser et al 2011):

$$\nu_{n_p,l} = \left(n_p + \frac{l}{2} + \varepsilon - \delta\nu_{0l} + \frac{\alpha}{2}(n_p - n_{\max})^2\right)\Delta\nu, \quad (3.3.3)$$

where the parameter α is the gradient

$$\alpha = \frac{d\log(\Delta\nu)}{dn}$$

The other quantities the expression (3.3.3) are already defined in the preceding subparagraphs. Using the frequencies and the radial orders of l=0 modes reported in Table 1 we obtained the value $\alpha = 0.00676$. This value is very close to value $\alpha = 0.00698$ obtained using the fit $\alpha = 0.015\Delta\nu^{-0.32}$, proposed by Moser et al. (2012).

We calibrated the model of rotational splitting expressed by (3.3.1) and (3.3.2) with our observational data by finding the values of the parameters λ and β such that the computed splittings match best the observed ones (see Table 2). The goodness of fit was quantified by the classical χ^2 minimization, $\chi^2 = \frac{1}{n}\sum_{i=1}^{n}(\delta\nu_i^{obs} - \delta\nu_i^{calc})^2$, where n=19 is the number of the fitted splittings. The fit returned the values $\lambda = 0.37$ and $\beta = 0.07$. We remark that the values of λ and β are very close to 0.5 and 0.08, respectively as it was expected according to Mosser et al. (2012). This may be regarded as a new confirmation of the practical applicability of the proposed model as an automated method for measuring the rotational splittings of dipole mixed modes (see Table 2).

Table 2. The calculated values of the rotational splittings, $\delta\nu_i^{calc}$, using the model proposed by Mosser et al. (2012) that match best the measured rotational splittings, $\delta\nu_i^{obs}$. All the values are in μHz.

$\nu_{l=1,m=0}$	$\delta\nu_i^{obs}$	$\delta\nu_i^{calc}$

116.29	0.225	0.230
117.32	0.221	0.213
118.14	0.155	0.166
118.82	0.175	0.166
119.77	0.227	0.217
120.85	0.235	0.232
126.80	0.237	0.233
128.02	0.218	0.218
129.03	0.149	0.164
129.77	0.171	0.172
130.89	0.216	0.223
137.82	0.237	0.232
139.23	0.211	0.210
140.15	0.158	0.154
141.23	0.200	0.205
149.42	0.228	0.229
150.66	0.192	0.188
151.68	0.176	0.169
153.08	0.228	0.226

4. STELLAR MODELING

The basic parameters of KIC006144777 are found using the asteroseismic inversion method. We have identified a best fit model for KIC006144777 by matching stellar models both to oscillation data and known observables. We take the effective temperature ($T_{eff} = 4677 \pm 200K$), the surface gravity ($\log g = 2.887 \pm 0.5 dex$), and the surface metallicity ([Fe/H]=-0.062 ± 0.5) from the *Kepler* Input Catalogue (KIC; Brown et al. 2011). We computed radial and nonradial oscillation frequencies of models distributed along the giant branch of evolutionary tracks in the HR diagram. The models were constructed with the CESAM2k stellar evolution code (Morel, 1997) for stellar masses from 0.75 to 1.35 $M_{\odot}$ with the step 0.02 $M_{\odot}$, refined to 0.001 $M_{\odot}$ localy in a vecinity of the point where the best fitting model is located, for initial helium content Y=0.26, 0.27, and 0.28 and initial metallicity Z=0.04, 0.03, 0.02, 0.01, 0.005, and 0.004, adopting OPAL96 opacity tables (Iglesias &Rogers, 1996), OPAL2001 equation of state (Rogers & Nayfonov, 2002), and NACRE reaction rates (Angulo et al. 1999). Diffusion of helium and heavy elements was not included. The convection is treated in the framework of the mixing length theory (Bohm-Vitense, 1958, Henyey et al. 1965) and the mixing length parameter is considered free parameter in the range 1.0 and 2.2 times the pressure scale height, with the step 0.02 times the pressure scale height, and no core overshooting.

The model eigenspectra is generated by ROMOSC linear, non-radial, non-adiabatic stellar pulsation code (Suran et al. 2001). This code is calibrated with the

corresponding ESTA stellar pulsation codes. In our analysis we only considered the radial modes and the non-radial modes with mode degree l up to 3. Following Jiang et al. (2011), we did not find it necessary to apply an offset to the model frequencies to correct for near-surface effects (Kjeldsen et al. 2008).

As usual, we quantify the difference between observed and calculated spectrum by the following χ^2 definition:

$$\chi^2 = \frac{1}{N}\sum_{i=1}^{N}\frac{\left(\nu_i^{\mathrm{obs}} - \nu_i^{\mathrm{calc}}\right)^2}{\sigma_i^2},$$

where ν_i^{obs} is the observed frequency for the i^{th} mode, ν_i^{calc} is the corresponding model frequency for the i^{th} mode, σ_i^2 is the observational uncertainty for the i^{th} mode and N is the total number of matched modes. In the case of red giants, it is difficult to identify a best fitting stellar mode that fit simultaneously all the radial and non-radial mixed modes (see e.g. Di Mauro et al. 2011; Jiang et al. 2011). In the case of the rotating red giant KIC 6144777, the modelling is more complicated because of the rotational splitting of the (closely spaced) l=1 mixed modes.

We have begun by fitting only the radial modes having the same radial order n, mainly because they are not splitted by the stellar rotation. We was able to identify an best fitting stellar model for KIC006144777 with mass M=0.845 $M_{\odot}$, effective temperature Teff=4477.5K, surface gravity logg=2.929dex, stellar radius R=5.22$R_{\odot}$, luminosity L=9.78$L_{\odot}$, chemical composition X=0.716, Y=0.28 and Z=0.004 (or [Fe/H]=-0.43 with respect to the solar metallicity [Grevesse & Noels 1993]), mixing length parameter $\alpha_{MLT} = 1.04$ and age=11.98Gyr. We note here that this and only this stellar model succeed to find in the 1σ uncertainty all of the l=0 and 2 modes and 16 of the l=1, m=0 and 3 of the l=3 observed modes (see Table 3).

Table 3. Calculated radial and non-radial strongly trapped unstable (STU) modes with the mode degree l up to 3 modes having the inertia equal or close to minima mode inertia. Only the calculated l=2 and 3 modes having minima mode inertia are considered.

l	n	ν[μHz]
0	8	102.66
0	9	113.06
0	10	123.65
0	11	134.39
0	12	145.17
0	13	156.03
1	7	96.62
1	7	97.65
1	8	107.70
1	9	116.64
1	9	118.27
1	9	119.36

1	9	121.42
1	10	126.04
1	10	128.26
1	10	129.45
1	11	131.30
1	11	138.83
1	11	140.17
1	11	142.18
1	12	150.20
1	12	151.52
1	12	154.21
1	13	161.87
1	13	164.35
2	8	111.84
2	9	122.49
2	10	133.13
2	11	144.18
2	12	155.13
3	9	125.89
3	10	136.79
3	11	147.42

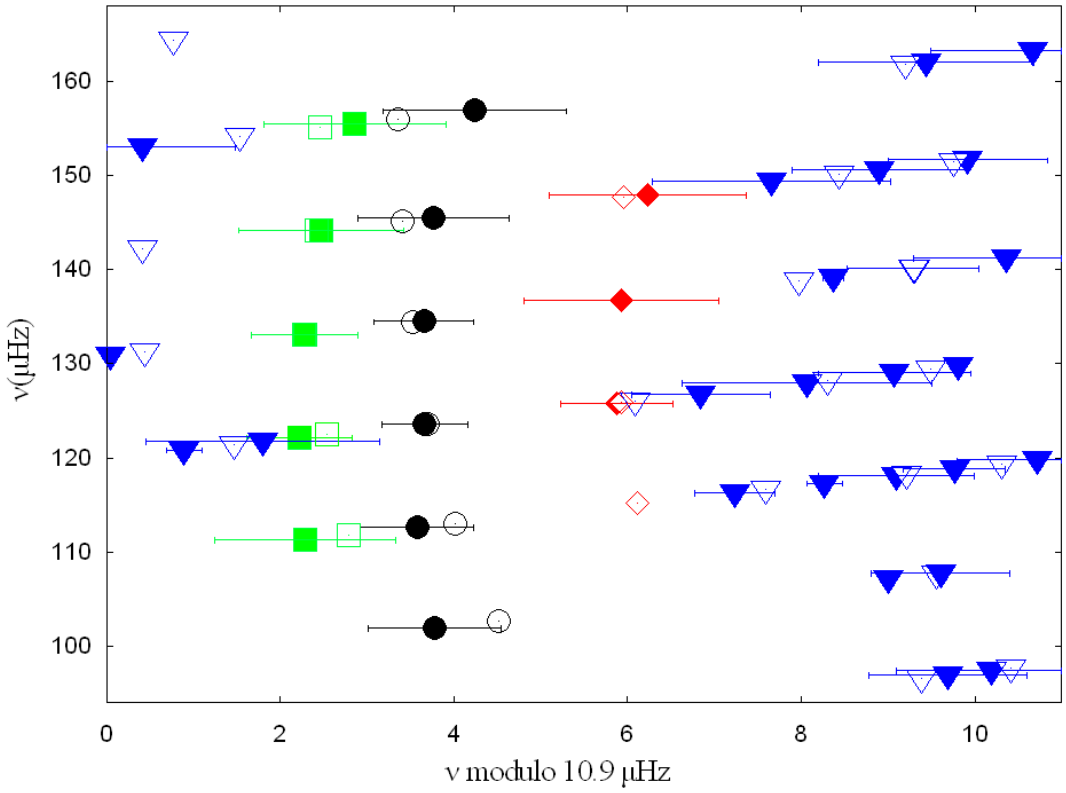

Figure 5. The échelle diagram based on observed and computed frequencies, plotted with $\Delta\nu = 10.9$ μHz. The open symbols represent computed frequencies, while the filled symbols represent observed frequencies of Table 3. Circles are used for modes with $l = 0$, triangles for $l = 1$, squares for $l = 2$, diamonds for $l = 3$.

Table 4. Calculated non-radial modes with the mode degree l=1 and radial order n, having minima of mode inertia, together with the frequencies corresponding to the centre of the l=1 ridge in the power spectrum, $\nu_{n_p,01} = \left(n_p + \frac{1}{2} + \varepsilon - \delta\nu_{01} \right) \Delta\nu$. The last column shows the frequencies of pure dipole p-modes, $\nu_{n_p,1}$, as expressed by (3.3.3).

l	n	ν[μHz]	$\nu_{n_p,01}$	$\nu_{n_p,1}$
1	7	97.65	96.63	96.96
1	8	107.70	107.54	107.68
1	9	118.27	118.44	118.48
1	10	129.45	129.35	129.35
1	11	140.17	140.25	140.29
1	12	151.52	151.16	151.30
1	13	161.87	162.06	162.39

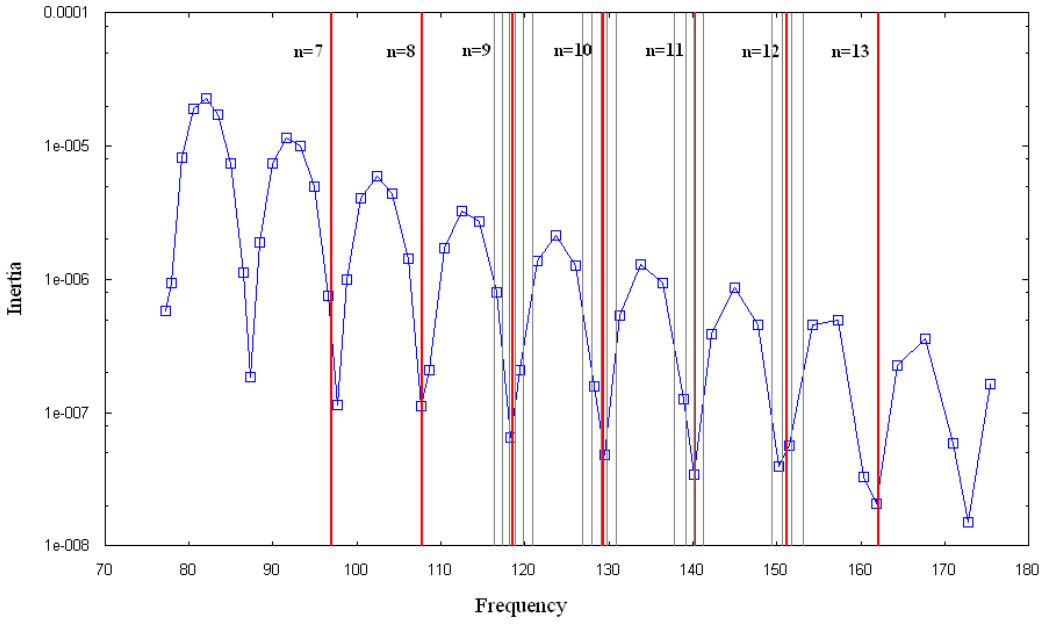

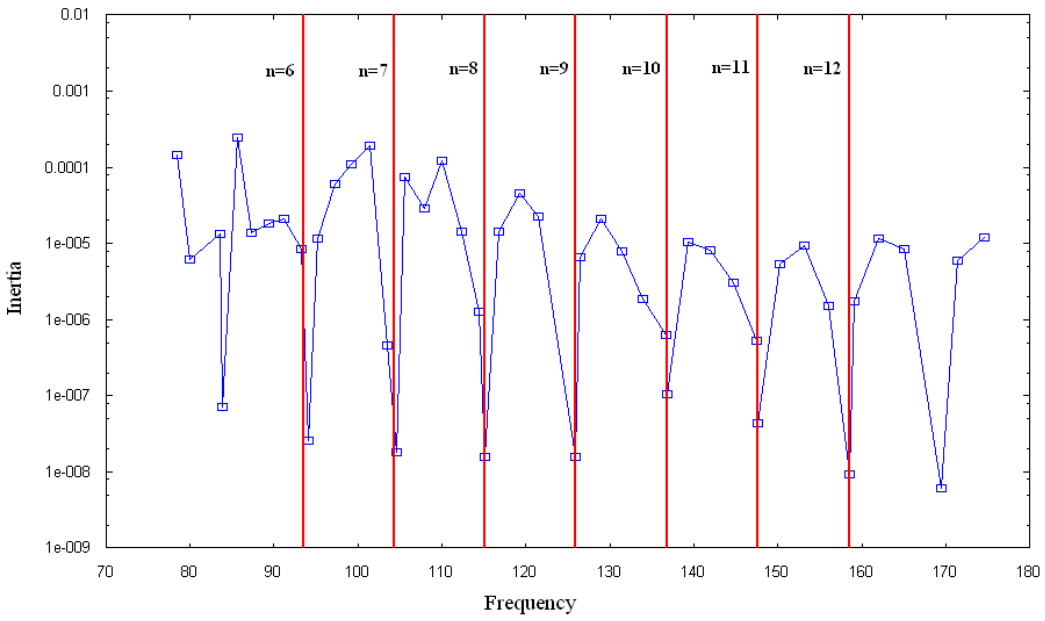

Fig.5. Calculated l=1 (top panel) and l=3 (bottom panel) modes. Vertical red lines represent the asymptotic frequencies $\nu_{n_p,l}$. Vertical grey lines in the top panel represent the frequencies $\nu_{l=1,m=0}$ listed in the first column of Table 2 (see also Fig. 6).

As mentioned in Section 3, we identified multiple l=1 mixed modes per radial order n (see Table 1). Some of them act like p-modes (p-dominated mixed modes) having a lower inertia than the g-dominated mixed modes, as discussed Beck et al. (2011) and Bedding et al. (2011). Measuring the period spacing for these observed mixed modes allow us to probe the cores of red giants stars (apj_142). Bedding et al. (2011) have found a way to distinguish between hydrogen-shell-burning and helium-burning red giants by using their different period spacing: the hydrogen-shell-burning stars have observed period spacing mostly around 50s, while the stars with helium-burning cores have observed period spacing of about 100 – 300s (see apj). Christensen-Dalsgaard (2011) also has found that measuring the period spacings may provide a method to determine the size of the convective core of those helium-burning red giants. The mean period spacing of KIC 006144777 is $60.975 \pm 2.674s$ which we measured by means of the power spectrum method (Bedding et al. 2011). This confirms that KIC006144777 is still in hydrogen-shell-burning phase. This value also agrees with our stellar model.

4.1. LINKING THE ROTATION SPLITTING TO THE CORE ROTATION

Following Mosser et al (2012), we qualitatively linked the observed rotational splittings of the dipole mixed p-modes (see Chapter 1) to the rotation inside the red giant star KIC006144777. We assume that the stellar rotation is slow enough that the first-order perturbation theory is sufficient to compute the rotational splittings. This theory yields the following expression for the rotational splittings (Ledoux 1951, Christensen-Dalsgaard & Frandsen 1983; Christensen-Dalsgaard & Berthomieu 1991; Goupil 2009; Goupil et al. 2012):

$$\delta\nu_{\mathrm{rot,n,l}} = \int_0^1 K_{n,l}(x)\frac{\Omega(x)}{2\pi}dx, \quad (3.1)$$

where $x = r/R$ is the normalized ratio and Ω is the angular rotation (in rad/s).The rotation kernel, $K_{n,l}$, of the mode of radial order n and angular degree l takes the form

$$K_{n,l} = \frac{1}{\mathrm{I_{n,l}}}\left[\xi_r^2 + (\Lambda - 1)\xi_h^2 - 2\xi_r\xi_h\right]_{\mathrm{n,l}} \rho x^2, \quad (3.2)$$

where $\mathrm{I_{n,l}}$ denotes the mode inertia:

$$\mathrm{I_{n,l}} = \int_0^1 \left(\xi_r^2 + \Lambda\xi_h^2\right)_{\mathrm{n,l}} \rho x^2 dx \quad (3.3)$$

The quantities ξ_r and ξ_h are the fluid vertical and horizontal displacement eigenfunctions, ρ is the density and $\Lambda = l(l+1)$.

With the two codes, CESAM2k and ROMOSC, we have estimated the rotational kernels in the best fitting stellar model for KIC6144777. The contribution of different regions of stellar interior to the rotational splitting can be quantified by the normalized integrated rotational kernels $\int_0^{x_c} K_{n,l}(x)dx / \int_0^1 K_{n,l}(x)dx$, where x_c=0.005245 correspond to core radius. The values of normalized integrated rotational kernels of few l=1 modes at the core boundary are listed in Table 5 together with the normalized mode inertia, $\mathrm{I_{n,l}}/(GM^2/R^3)$. We clearly see that the values of the normalized integrated rotational kernels at the core boundary are proportional with the mode inertia. This is in agreement with our expectations if we have in view that the mixed p-modes have higher amplitude in the central regions as the mode inertia is higher, while the amplitudes in the outer regions are almost the same. Consequently, the contribution of core rotation to the rotational splittings of the mixed modes increases as the mode inertia increases. Figure 6 shows the normalized integrated rotational kernels derived for four dipole mixed p-modes with minima mode inertia and having the frequencies 118.27 μHz, 129.45 μHz, 140.17 μHz, and 150.20 μHz. We see that the kernels in the p-m modes are less dominated by the core since they reach a value less than 0.62 at the core boundary (see also Table 5). Figure 7 shows the normalized integrated kernels of the g-m modes of ν=126.04 μHz, ν=128.26 μHz, and ν=131.30 μHz. We see that the kernels in the g-m modes are dominated by the core, since the normalized integrated kernels reach a value larger than 0.75 at the core boundary (see also Table 5).

Table 5. The normalized integrated rotational kernels and the normalized mode inertia for few l=1 p-m and g-m modes with the frequency ν.

ν [μHz]	$\int_0^{x_c} K_{n,l}(x)dx / \int_0^1 K_{n,l}(x)dx$	$\mathrm{I_{n,l}}/(GM^2/R^3)$ [$\times 10^{-7}$]
118.27	0.618	0.649
126.04	0.844	12.589
128.26	0.757	1.591
129.45	0.580	0.484
131.30	0.817	5.400
140.17	0.523	0.343
150.20	0.582	0.394

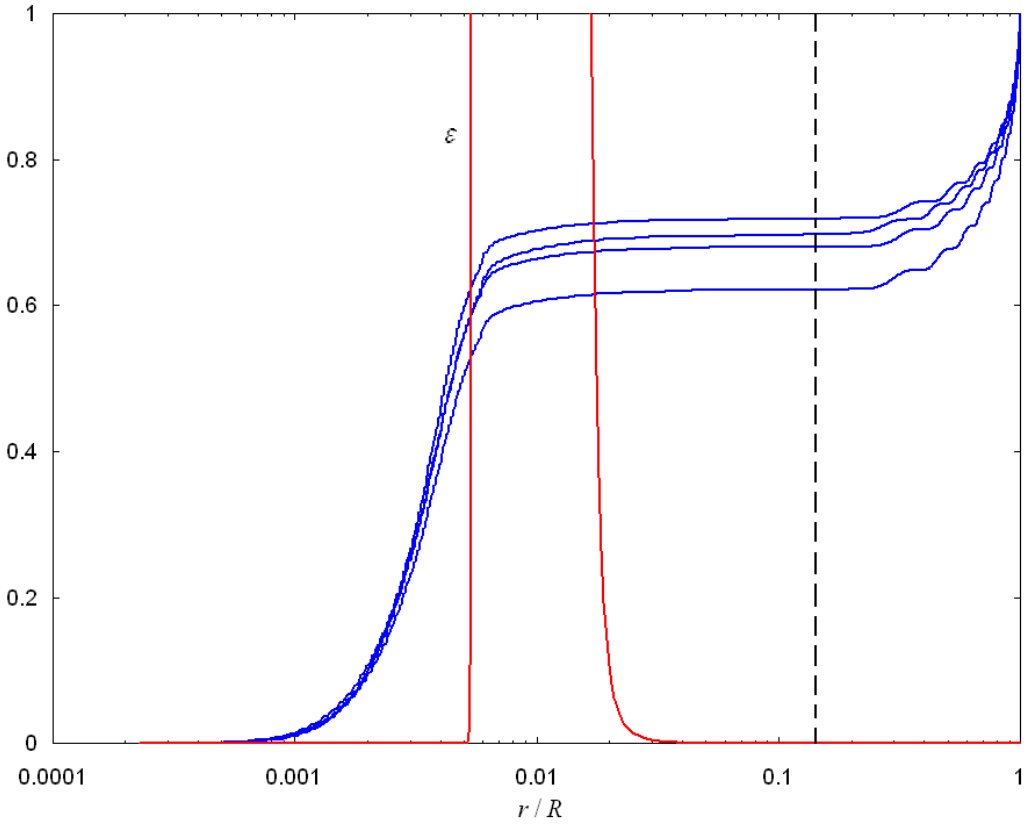

Fig. 6. The normalized integrated rotational kernels $\int_0^{x_c} K_{n,l}(x)dx / \int_0^1 K_{n,l}(x)dx$ (blue) for the l=1 modes in the frequency range [118.27, 150.2] μHz, having minima mode inertia (see the text) in the best fitting stellar model for KIC006144777. The values of these kernels at the core boundary are proportional with the mode inertia. Dashed line marks the base of the convective envelope, located at $x_{\mathrm{conv}} = 0.142$. The red line represents the thermonuclear energy generation rate ε.

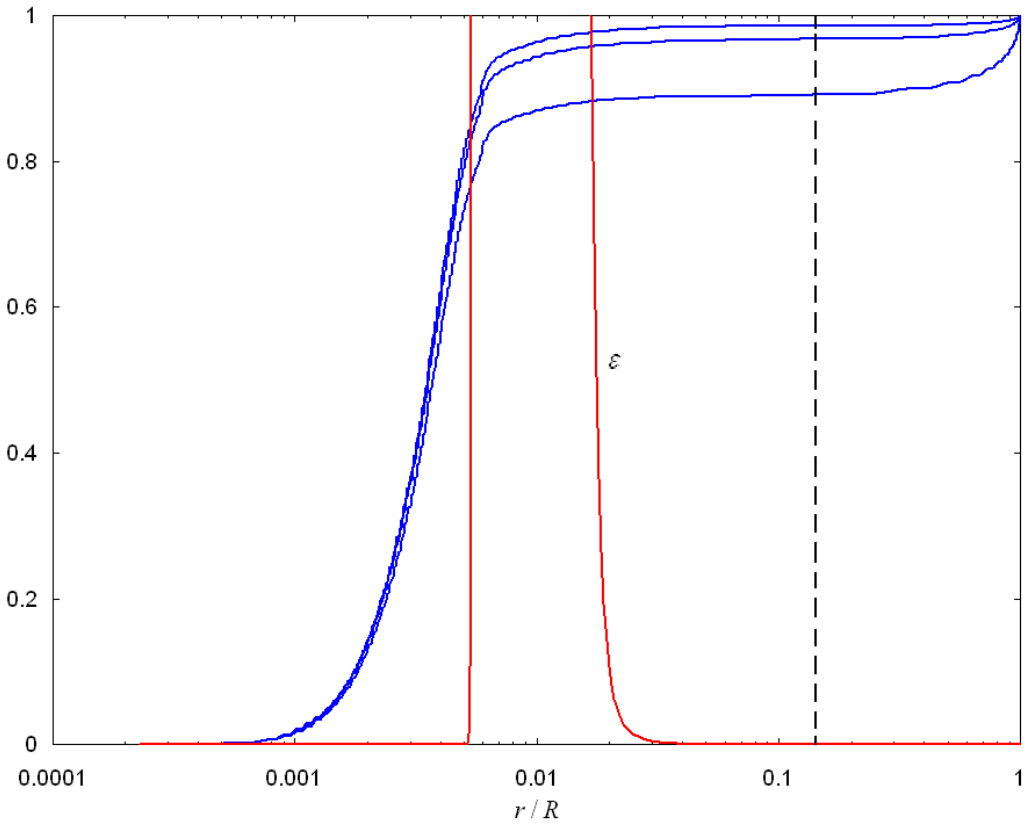

Fig. 7. The normalized integrated rotational kernels for three g-m modes of frequencies: ν=126.04 μHz, ν=128.26 μHz, and ν=131.30 μHz. The red line and the dashed line represent the thermonuclear energy generation rate ε and the base of the convective envelope, respectively.

4.2 THE PROFILE OF INTERNAL ROTATION

In this paper we adopted the following expression to describe the internal stellar rotation (Lee & Saio, 1993):

$$\Omega(x) = \Omega_s \left[1 + \frac{b-1}{1+e^{a(x-x_c)}} \right] \quad (4.1)$$

where a, b are real and $b>1$, Ω_s is the angular rotation at stellar surface. The other quantities are already defined. We remark that, for $b>1$ the core rotation is faster than the envelope rotation, and the angular rotation have a steep decrease at the core boundary while it is almost constant in the core (see Lee (1988) for some examples). The angular rotation at the core boundary is

$$\Omega_c = \Omega(x_c) = \Omega_s (1+b)/2 \quad (4.2)$$

Using the relation (4.2) between Ω_c and Ω_s, the expression (4.1) for the internal stellar rotation can be written as follows:

$$\Omega(x) = \frac{2\Omega_c}{1+b}\left[1 + \frac{b-1}{1+e^{a(x-x_c)}}\right] \quad (4.3)$$

In that following we propose to find the internal rotation profile that match best the calculated and the observed splittings of the l=1 modes of our stellar model with the frequencies between 116 μHz and 152 μHz. By calculated splitting we denoted the frequency splitting as is computed with the formula (3.1) where $\Omega(x)$ is given by expression (4.3). On the other hand, we have seen (Cap. 3) that the observed rotational splittings of the dipole mixed modes can be also computed with high accuracy using the asymptotic formula (3.3.1) that were calibrated with the measured splittings. Based on this idea, we have estimated the 'observed' splittings of our fitted modes using (3.3.1) and (3.3.2) (see Table 6), in which $\nu_{n_p,l}$ was replaced by the corresponding model frequency having minima inertia and the same radial order. We considered a 3D grid with a from 1 to 100 with the step 1, b from 10 to 10^6 with the step 10, and x_c from 2.27×10^{-4} to 5.55×10^{-3} with the step 4.07×10^{-5} (more precisely, for x_c we have considered the first 120 central shells of the stellar model as it was constructed with CESAM2k code). In the fitting, the parameter Ω_c is set to a value estimated using the following asymptotic expression for the rotational splittings, valid for g-m modes (Mosser et al. 2012):

$$\delta\nu_{rot} \approx \frac{1}{2}\frac{\langle\Omega\rangle_{core}}{2\pi} \quad (4.4)$$

where

$$\langle\Omega\rangle_{core} = \frac{\int_0^{x_c} K_{n,l}(x)\Omega(x)dx}{\int_0^{x_c} K_{n,l}(x)dx}.$$

If we replace $\delta\nu_{rot}$ in (4.4) by its observed value 0.237 μHz (see Cap 3, Table 2) we obtain $\langle\Omega\rangle_{core} \approx 0.948\pi\times10^{-6}\,rad/s$. According to this value and having in mind that the rotation is almost constant in the core, we have set the value of Ω_c to $0.94\pi\times10^{-6}\,rad/s$ (corresponding to a period of 24.626 days). The best fitting internal rotation profile minimize the quantity $\chi^2_{\delta\nu} = (1/N)\sum_{i=1}^{N}(\delta\nu_i^{calc} - \delta\nu_i^{obs})^2$ while we search on the above mentioned 3D grid. The fit returned values of $a = 28\pm1$, $b = 920600.8\pm10$ and $x_c = 4.045\times10^{-3}\pm4.07\times10^{-5}$, where the uncertainties are given by the grid resolution. Using (4.2) we have computed the angular rotation at surface, $\Omega_s = 2.042\pi\times10^{-12}\pm2\pi\times10^{-17}$ rad/s. This corresponds to a period of 31036 years! The internal rotation profile (Figure 8) shows us a strong differential rotation. The angular rotation is $3.947\pi\times10^{-8}\,rad/s$ (corresponding to a period of 1.6 years) at the base of the convective envelope while it is almost equal to Ω_s for $x \geq 0.6$ (the

convective envelope has rigid rotation for $r \geq 0.6R$). Brun & Palacios (2009) also found differential rotation in the convective envelope of red giants based on 3-D simulations. Thus, the angular momentum is transferred from core to the envelope and the mean core rotation slows down (Mosser et al 2012; Marques et al 2012; Goupil et al 2012). Moser et al. (2012) concluded that this spinning down during the red giant phase explains, for instance, the long rotation periods measured in white dwarfs.

Table 6. Values of the rotational splitings, δν_obs, as they are estimated using the asymptotic formula (*) for few l=1 modes, ν(calc), of the stellar model. Last column shows the fitted values of these splittings, δν_calc, if the internal rotation profile is given by the expression (4.1).

l	n	ν(calc)	δν_obs(μHz)	δν_calc(μHz)
1	9	116.64	0.224	0.227
1	9	118.27	0.151	0.189
1	9	119.36	0.211	0.217
1	9	121.42	0.235	0.227
1	10	126.04	0.236	0.228
1	10	128.26	0.214	0.215
1	10	129.45	0.151	0.183
1	10	131.30	0.227	0.225
1	10	133.78	0.237	0.227
1	11	136.36	0.237	0.226
1	11	138.83	0.218	0.211
1	11	140.17	0.151	0.171
1	11	142.18	0.229	0.222
1	11	144.93	0.238	0.224
1	12	147.77	0.232	0.222
1	12	150.20	0.151	0.183
1	12	151.52	0.218	0.197
1	12	154.21	0.237	0.222

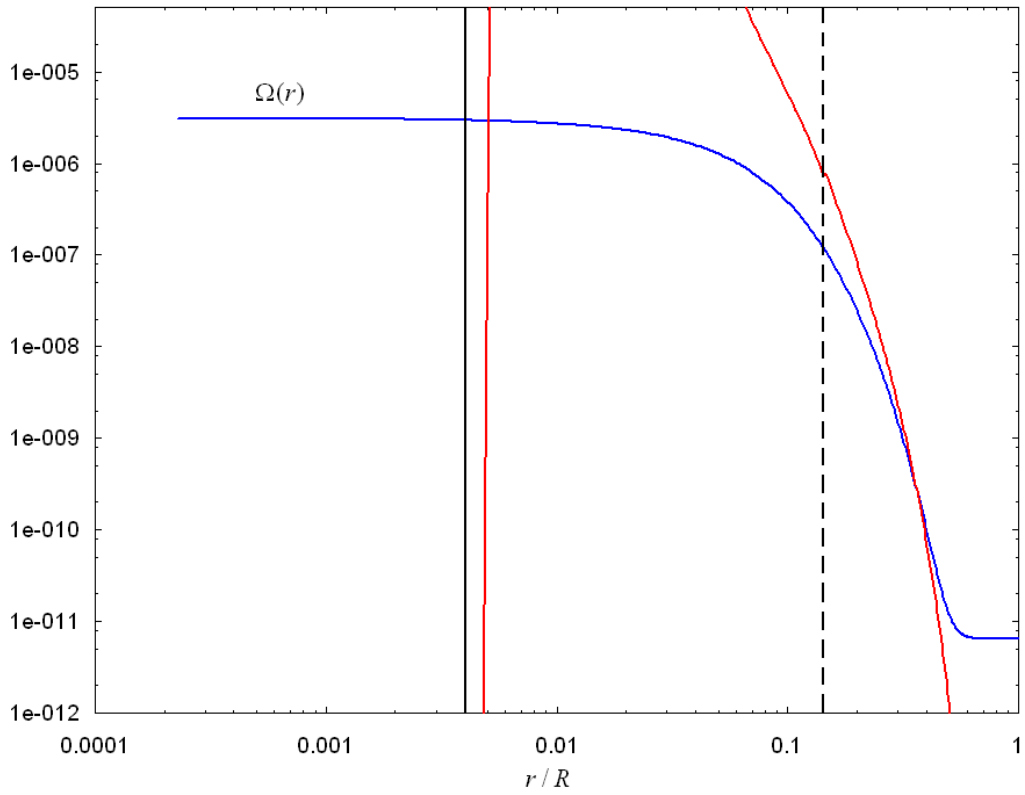

Fig. 8. Internal differential rotation profile (blue). Logarithmic scale was used on both axes. The vertical black line marks the boundary, x_c, of the rigid rotating core. The red line and the dashed line represent the thermonuclear energy generation rate ε and the base of the convective envelope, respectively.

5. CONCLUSION

In this paper we have analyzed the time-series data sets of the star KIC006144777 from Kepler to extract its oscillation parameters. Some l=1 modes shows obvious rotational splitting. We have measured the rotational splitting of 16 l=1 modes in the range between 116 μHz and 155 μHz and we have found the value of the maximum observed splitting in the g-m mixed modes $\delta\nu_{\mathrm{rot}} = 0.237\mu\mathrm{Hz}$. Based on this value we have estimated the period of the core rotation $\mathrm{T_{core}} \approx 24\ \mathrm{days}$.We also have found that the asymptotic expression proposed by Mosser et al. (2011) for estimation of the rotational splittings of mixed modes is also valid in the case of KIC006144777 with values of the parameters $\lambda = 0.37$ and $\beta = 0.07$, very close to those proposed by Mosser et al. (2011). By using the scaling relations between $\Delta\nu$, ν_{max}, and the stellar effective temperature $\mathrm{T_{eff}}$ we estimated the stellar mass as $1.28 \pm 0.16\mathrm{M_{Sun}}$. The powerful method of matching stellar models both to oscillation data and known observables of KIC 6144777 was applied in order to determine the stellar global physical parameters more accurately. We have searched for models in a large range because the scaling relations, and hence the estimated mass, are not so reliable for the giant branch stars (Stello et al. 2008). The best fitting stellar model has found to have a mass of 0.845 $\mathrm{M}_{\odot}$ and Z=0.004. Furthermore, parameters such as effective temperature, surface gravity, radius, luminosity, and age are also determined after comparison. The internal differential rotation profile and the boundary of the rigid

rotating core was found by comparing the rotational splittings of l=1 modes of the best stellar model as computed in the frame of the perturbation theory of the first order with the rotational splittings of the same modes as estimated by using the asymptotic expression of Mosser et al (2011). We also obtained the observed mean period spacing of $l = 1$ modes with a value of 61 ± 2.67 s. From the modelled evolutionary track of KIC006144777, we know it is in the hydrogen-shell-burning phase and on the ascending giant branch, which is consistent with the results of Bedding et al. (2011) on the mean period spacing of mixed modes for red giants.

REFERENCES

*Aerts, C., Christensen-Dalsgaard, J., & Kurtz, D.W. (ed.) 2010, Asteroseismology (Berlin: Springer)
*Aizenman, M., Smeyers, P., & Weigert, A. 1977, A&A, 58, 41
*Angulo, C., Arnould, M., Rayet, M., et al. 1999, Nucl. Phys. A, 656, 3
*Appourchaux, T. 2003, A&A, 412, 903
*Barban, C., Matthews, J. M., De Ridder, J., et al. 2007, A&A, 468, 1033
*Beck, P. G., Bedding, T. R., Mosser, B., et al. 2011, Science, 332, 205
*Bedding, T. R., Huber, D., Stello, D., et al. 2010, ApJ, 713, L176
*Bedding, T. R., & Kjeldsen, H. 2003, PASA, 20, 203
*Bedding, T. R., Mosser, B., Huber, D., et al. 2011, Nature, 471, 608
*B¨ohm-Vitense, E. 1958, Z. Astrophys., 46, 108
*Borucki, W., Koch, D., Basri, G., et al. 2008, in IAU Symp. 249, Exoplanets: Detection, Formation and Dynamics, ed. R. Dvorak (Cambridge: Cambridge Univ. Press), 17
*Borucki, W. J., Koch, D., Basri, G., et al. 2010, Science, 327, 977
*Brown, T. M., Gilliland, R. L., & Noyes, R. W. 1991, ApJ, 368, 599
*Brown, T. M., Latham, D.W., Everett, M. E., & Esquerdo, G. A. 2011, AJ, 142, 112
*Buzasi, D., Catanzarite, J., Laher, R., et al. 2000, ApJ, 532, L133
*Carrier, F., De Ridder, J., Baudin, F., et al. 2010, A&A, 509, A73
*Chaplin, W. J., Appourchaux, T., Elsworth, Y., et al. 2010, ApJ, 713, L169
*Chaplin, W. J., Bedding, T. R., Bonanno, A., et al. 2011, ApJ, 732, L5
*Christensen-Dalsgaard, J. & Frandsen, S. 1983, Sol. Phys., 82, 469
*Christensen-Dalsgaard, J. & Berthomieu, G. 1991, Theory of solar oscillations, ed. Cox, A. N., Livingston, W. C., & Matthews, M. S. (Tucson, AZ, University of Arizona Press), 401–478
*Christensen-Dalsgaard, J. 2004, Sol. Phys., 220, 137
*Christensen-Dalsgaard, J. 2011, in Asteroseismology: Canary Islands Winter School of Astrophysics, Vol. XXII, ed. P. Pall´e (Cambridge: Cambridge Univ. Press), in press (arXiv:1106.5946)
*Christensen-Dalsgaard, J., Arentoft, T., Brown, T. M., et al. 2007, Commun. Asteroseismol., 150, 350
*De Ridder, J., Barban, C., Baudin, F., et al. 2009, Nature, 459, 398
*De Ridder, J., Barban, C., Carrier, F., et al. 2006, A&A, 448, 689
*Deheuvels, S., et al. 2010, A&A, 515, A87
*Di Mauro, M. P., Cardini, D., Catanzaro, G., et al. 2011, MNRAS, 415, 3783

*Dupret, M.-A., Belkacem, K., Samadi, R., et al. 2009, A&A, 506, 57
*Dziembowski, W. A., Gough, D. O., Houdek, G., & Sienkiewicz, R. 2001, MNRAS, 328, 601
*Edmonds, P. D., & Gilliland, R. L. 1996, ApJ, 464, L157
*Frandsen, S., Carrier, F., Aerts, C., et al. 2002, A&A, 394, L5
*Gilliland, R. L. 2008, AJ, 136, 566
*Gilliland, R. L., Brown, T. M., Christensen-Dalsgaard, J., et al. 2010, PASP, 122, 131
*Gizon, L., Ballot, J., Michel, E. 2013, Proceedings of the National Academy of Sciences, vol. 110, issue 33, pp. 13267-13271
*Gough, D. O. 1986, in Hydrodynamic and Magnetodynamic Problems in the Sun and Stars, ed. Y. Osaki (Tokyo: Univ. of Tokyo Press), 117
*Guenther, D. B., Demarque, P., Buzasi, D., 2000, ApJ, 530, L45
*Goupil, M., Belkacem, K., Marques, J., et al. 2012, A&A, 548A, 10M
*Goupil, M. J. 2009, in Lecture Notes in Physics, Berlin Springer Verlag, Vol. 765, The Rotation of Sun and Stars, 45–99
*Hekker, S., Elsworth, Y., De Ridder, J., et al. 2011b, A&A, 525, A131
*Hekker, S., Gilliland, R. L., Elsworth, Y., et al. 2011a, MNRAS, 414, 2594
*Hekker, S., Kallinger, T., Baudin, F., et al. 2009, A&A, 506, 465
*Huber, D., Bedding, T. R., Stello, D., et al. 2010, ApJ, 723, 1607
*Iglesias, C. A., & Rogers, F. J. 1996, ApJ, 464, 943
*Jenkins, J.M., Caldwell, D. A., Chandrasekaran, H., et al. 2010, ApJ, 713, L120
*Jiang, C., Jiang, B. W., Christensen-Dalsgaard, J., et al. 2011, ApJ, 742, 120
*Kallinger, T., Guenther, D. B., Matthews, J. M., et al. 2008a, A&A, 478, 497
*Kallinger, T., Guenther, D. B., Weiss, W. W., et al. 2008b, Commun. Asteroseismol., 153, 84
*Kallinger, T., Mosser, B., Hekker, S., et al. 2010, A&A, 522, A1
*Karoff, C. 2008, PhD thesis, Department of Physics and Astronomy, Univ. Aarhus
*Kjeldsen, H., & Bedding, T. R. 1995, A&A, 293, 87
*Kjeldsen, H., Bedding, T. R., & Christensen-Dalsgaard, J. 2008, ApJ, 683, L175
*Koch, D. G., Borucki,W. J., Batalha, N., 2010, AAS, 42, 302
*Ledoux, P. 1951, ApJ, 114, 373
*Lee, U.: 1988, *MNRAS*, **232**, 711
*Lee, U., Saio, H.: 1993, *MNRAS*, **261**, 415
*Lenz, P., & Breger, M. 2004, in IAU Symp. 224, The A-Star Puzzle, ed. J. Zverko, J. Ziznovsky, S. J. Adelman,&W.W.Weiss (Cambridge: Cambridge Univ. Press), 786
*Morel, P. 1997, A&AS, 124, 597
*Mosser, B., Belkacem, K., Goupil, M. J., et al. 2010, A&A, 517, A22
*Mosser, B., Belkacem, K., Goupil, M. J., et al. 2011, A&A, 525, L9
*Mosser, B.,. Goupil, M.J., Belkacem, K., et al. 2012, A&A, 548A, 10M
*Osaki, J. 1975, PASJ, 27, 237
*Retter, A., Bedding, T. R., Buzasi, D. L., Kjeldsen, H., & Kiss, L. L. 2003, ApJ, 591, L151
*Rogers, F. J., & Nayfonov, A. 2002, ApJ, 576, 1064
*Stello, D., Bruntt, H., Kjeldsen, H., et al. 2007, MNRAS, 377, 584
*Stello, D., Bruntt, H., Preston, H., & Buzasi, D. 2008, ApJ, 674, L53
*Stello, D., & Gilliland, R. L. 2009, ApJ, 700, 949
*Şuran, M.D., Goupil, M., Baglin, A., Lebreton, Y., Catala, C.: 2001, *A&A.*, **372**, 233
*Tarrant, N. J., Chaplin, W. J., Elsworth, Y., Spreckley, S. A., & Stevens, I. R. 2007, MNRAS, 382, L48

*Tassoul, M. 1980, ApJS, 43, 469